# Effect of electron- and hole-doping on properties of kagomé-lattice ferromagnet Fe<sub>3</sub>Sn<sub>2</sub>

Milo Adams<sup>1</sup>, Chen Huang<sup>2,3,4,\*</sup> and Michael Shatruk<sup>1,3,4,\*</sup>

E-mail: shatruk@chem.fsu.edu and chuang3@fsu.edu

Received xxxxxx Accepted for publication xxxxxx Published xxxxxx

### **Abstract**

We report a theoretical investigation of effects of Mn and Co substitution in the transition metal sites of the kagomé-lattice ferromagnet,  $Fe_3Sn_2$ . Herein, hole- and electron-doping effects of  $Fe_3Sn_2$  have been studied by density-functional theory calculations on the parent phase and on the substituted structural models of  $Fe_{3-x}M_xSn_2$  (M = Mn, Co; x = 0.5, 1.0). All optimized structures favor the ferromagnetic ground state. Analysis of the electronic density of states (DOS) and band structure plots reveals that the hole (electron) doping leads to a progressive decrease (increase) in the magnetic moment per Fe atom and per unit cell overall. The high DOS is retained nearby the Fermi level in the case of both Mn and Co substitutions. The electron doping with Co results in the loss of nodal band degeneracies, while in the case of hole doping with Mn emergent nodal band degeneracies and flatbands initially are suppressed in  $Fe_{2.5}Mn_{0.5}Sn_2$  but re-emerge in  $Fe_2MnSn_2$ . These results provide key insights into potential modifications of intriguing coupling between electronic and spin degrees of freedom observed in  $Fe_3Sn_2$ .

Supplementary material for this article is available online

Keywords: band structure, ferromagnetism, kagomé lattice

(Some figures may appear in colour only in the online journal)

# 1. Introduction

The kagomé lattice has served as one of the main testbeds for studies on the physics of spin frustration [1,2], allowing fundamental theoretical and experimental insights into such unconventional states of matter as spin ice [3] and spin liquid [3,4]. Pairwise antiferromagnetic (AFM) interactions between nearest neighbors cannot be simultaneously satisfied in the kagomé-lattice arrangement of magnetic moments [5], as AFM alignment of two spins on a single triangle leads to

ambiguous orientation of the third spin on the same triangle, thus disrupting magnetic ordering [6]. Such frustration propagating through a solid-state lattice leads to fragile magnetism, i.e., even small external perturbations might have a strong effect on the long-range magnetic behavior across the periodic structure [7,8]. Thus, the kagomé-type materials hold great potential not only for insight into fundamental properties of spin-frustrated systems but also for practical applications in future spintronic devices with low-energy power consumption [9].

<sup>&</sup>lt;sup>1</sup> Department of Chemistry and Biochemistry, Florida State University, Tallahassee, FL 32306-4390, USA

<sup>&</sup>lt;sup>2</sup> Department of Scientific Computing, Florida State University, Tallahassee, FL 32306-4120, USA

<sup>&</sup>lt;sup>3</sup> Materials Science and Engineering Program, Florida State University, Tallahassee, FL 32310, USA

<sup>&</sup>lt;sup>4</sup> National High Magnetic Field Laboratory, Tallahassee, FL 32310, USA

The recent growth of research on topological materials has reinvigorated interest to the kagomé lattice due to its tendency to host unique electronic correlations [6,10]. The network of hexagons enclosed by corner-sharing triangles creates the topological condition for destructive interference of the electron wavefunctions around each hexagon. As a result, dispersionless flatbands are observed in the electronic band structure [11-14]. Charge carriers occupying these highly degenerate flatbands are rendered "superheavy" by selflocalization. Driven by these considerations, research efforts on kagomé lattices have ventured beyond AFM-correlated materials, as even ferromagnetic (FM) kagomé materials have been shown to exhibit intriguing topological properties [15]. For example, a giant anomalous Hall effect [16], massive Dirac fermions [17], and skyrmion bubbles [18] have been reported for the kagomé-lattice metal, Fe<sub>3</sub>Sn<sub>2</sub>. This material crystallizes in the filled NiAs structure type [19] (the space group  $R\overline{3}m$ ). The crystal structure features kagomé layers of Fe atoms alternating with hexagonal layers of Sn atoms, while additional Sn atoms center hexagons of the kagomé layer (Figure 1). A 2009 report classifying Fe<sub>3</sub>Sn<sub>2</sub> as a frustrated ferromagnet with the ordering temperature ( $T_{\rm C}$ ) of 640 K and temperature-dependent non-collinear spin texture [20], followed by the report of the giant anomalous Hall effect [16], spurred extensive studies of the electronic structure and topological properties of this material. Dirac cones at symmetry point K were revealed experimentally by ARPES measurements [17], while further analysis identified dispersionless flatbands at ~0.2 eV below the Fermi level along the  $\Gamma$ -K and  $\Gamma$ -M directions [21]. Isolation of these bands is of great interest for the realization of new magnetically driven fractionalized phases of matter. A possible approach to achieve this objective is to tune the electronic structure by chemical substitutions. Till now, however, essentially all studies of Fe<sub>3</sub>Sn<sub>2</sub> have focused on the pristine composition.

In this work, we report a theoretical evaluation of the effects of hole and electron doping on the magnetic properties and electronic structure of Fe<sub>3</sub>Sn<sub>2</sub>. These effects are achieved by partial replacement of Fe with Mn and Co, respectively. The compositional analogues, Mn<sub>3</sub>Sn<sub>2</sub> [22] and Co<sub>3</sub>Sn<sub>2</sub> [23], are known ferromagnets that belong to the orthorhombic Ni<sub>3</sub>Sn<sub>2</sub> structure type (space group *Pnma*), although the hightemperature modification of Co<sub>3</sub>Sn<sub>2</sub>, obtained by quenching from above 900 K, does exhibit the hexagonal filled NiAstype structure [23]. Effects of Fe for Mn substitution on the properties of Mn<sub>3</sub>Sn<sub>2</sub> were studied by Recour et al. in a report on magnetic and magnetocaloric properties of Fe<sub>3-x</sub>M<sub>x</sub>Sn<sub>2</sub> on the Mn-rich side  $(0.1 \le x \le 0.8)$  [24], but no such studies have been performed for the other limiting composition, i.e., when substituting Mn for Fe in Fe<sub>3</sub>Sn<sub>2</sub>. The present work, to the best of our knowledge, is the first attempt to explore possible effects of chemical substitutions on the properties of Fe<sub>3</sub>Sn<sub>2</sub>.

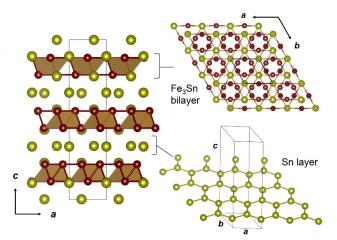


**Figure 1.** The crystal structure of Fe<sub>3</sub>Sn<sub>2</sub> viewed perpendicular to the *ac* plane (left) to reveal alternating Fe<sub>3</sub>Sn and Sn layers, shown on the right. The Fe<sub>3</sub>Sn slab is formed by stacking of two kagomé layers of Fe atoms, with the Sn atoms centering hexagons of each layer. In the image of the bilayer, the brighter and duller colors indicate atoms located in different kagomé layers.

### 2. Methods

Electronic structure calculations were performed at the density-functional theory (DFT) level with Quantum Espresso (version 7.0) [25], using scalar relativistic projectoraugmented wave pseudopotentials within the Perdew-Burke-Ernzerhof generalized gradient approximation (PBE-GGA) [26]. The self-consistent energy convergence criterion was set to  $10^{-6}$  eV, with a  $\Gamma$ -centered 8x8x8 k-point mesh. The reported unit cell and atomic parameters of Fe<sub>3</sub>Sn<sub>2</sub> were taken as the starting point for calculations [19]. Lattice relaxations were conducted with convergence thresholds of 0.5 kbar for pressure, 0.001 eV/Å for forces, and 10<sup>-5</sup> eV for the total energy per unit cell. Fermi-Dirac smearing was used with a smearing energy of 0.1 eV. The plane wave kinetic energy cutoff was set at 500 eV. A dense 16x16x16 k-point mesh was used to calculate the density of states. Crystal structure visualization and plotting were performed with VESTA [27].

The influence of hole- and electron-doping effects on the electronic structure of Fe<sub>3</sub>Sn<sub>2</sub> was modeled by partially substituting Mn and Co, respectively, for Fe. Since we are interested in perturbations of the electronic structure in the vicinity of the Fermi level, and since  $M_3Sn_2$  (M = Mn, Co) exhibit a different structure type, we have restricted these calculations to the smaller levels of substitution, i.e., to compositions Fe<sub>3-x</sub>M<sub>x</sub>Sn<sub>2</sub> with x = 0.5 and 1.0. To implement such models, the 30 atoms in the unit cell of Fe<sub>3</sub>Sn<sub>2</sub> were described as unique positions by lowering the symmetry to P1. Calculations performed on Fe<sub>3</sub>Sn<sub>2</sub> in both the original  $R\overline{3}m$  and the P1 space groups yielded comparable results, thus confirming the validity of such an approach.

#### 2. Results and Discussion

#### 2.1 Substitution models

Our initial DFT calculations on the unsubstituted Fe $_3$ Sn $_2$  revealed that the FM state is stabilized by 0.089 eV per unit cell relative to the paramagnetic (PM) state. The calculated magnetic moments were 2.24  $\mu_B$  per Fe atom and -0.08  $\mu_B$  per Sn atom, giving the total magnetic moment of 6.56  $\mu_B$  per formula unit (f.u.). These values are essentially the same as those reported recently by Fayyazi *et al.* [28]. They also compare well to the magnetic moment of 2.17  $\mu_B$  per Fe atom determined by neutron diffraction experiments at 10 K [29]. The most pronounced features of the band structure near the Fermi level are also commensurate with the previous reports, as will be discussed below in the section on the hole- and electron-doping effects.

Given the good agreement between our calculations and previous experimental and theoretical results on Fe<sub>3</sub>Sn<sub>2</sub>, we proceeded to calculating the electronic structures and magnetic properties of  $Fe_{3-x}M_xSn_2$  (M = Mn, Co; x = 0.5 and 1.0). To model such substitutions, we lowered the symmetry to P1 and confirmed that the electronic structure and magnetic parameters of Fe<sub>3</sub>Sn<sub>2</sub> remained essentially the same when calculated in this space group. Then, the substitution models were calculated for several random distributions of the Fe and M atoms, according to the desired compositions. The similar energies of different configurations, with the maximum energy difference of 7.1 µeV, confirmed that neither Mn nor Co atoms showed preference for a specific substitution pattern (Table S1). Subsequent calculations were performed using a single substitution pattern for each of the studied compositions; the pattern was chosen in such a way as to achieve the most random distribution of the Fe and M atoms (Figure S1 and Tables S2 and S3).

The optimized crystal structures showed that the replacement of Fe with Mn or Co led, respectively, to the increase and decrease in the unit cell volume (Table 1), in agreement with expectations based on the relative size of the transition metal atoms. The only exception is the small increase in the unit cell volume when going from Fe<sub>3</sub>Sn<sub>2</sub> to Fe<sub>2.5</sub>Co<sub>0.5</sub>Sn<sub>2</sub>. Interestingly, the hole- and electron-doping have different effects on the average distances between the transition metal atoms. The experimental Fe<sub>3</sub>Sn<sub>2</sub> structure has two types of such distances: there are shorter (2.590 Å) and longer (2.754 Å) Fe-Fe distances within the kagomé layer and the same shorter distance (2.590 Å) between the layers in the bilayer kagomé structure. Since we performed the crystal structure optimization without symmetry restrictions, we observe three different values for two shorter and one longer distances (Table 1). The calculated shorter *intra*layer distance shows a pronounced increase, from 2.551 Å to 2.623 Å, upon substitution of Mn for Fe but is less affected by the substitution of Co for Fe, varying between 2.537 Å and 2.575

Å. On the contrary, the shorter *inter* layer distance shows smaller changes, varying between 2.556 Å and 2.587 Å upon Mn doping and between 2.556 Å and 2.549 Å upon Co doping. Although the largest changes in the distances between transition metals appear to take place within the kagomé layer, the unit cell shows much larger changes along the c axis, i.e., perpendicular to the layers. This difference is explained by the pronounced changes in the distances between the transition metal and tin atoms along the c axis (Table S4).

**Table 1.** Unit cell parameters and interatomic distances in the optimized structures of Fe<sub>3-x</sub> $M_x$ Sn<sub>2</sub> (M = Mn, Co; x = 0.5, 1.0).

Camanasitian	Unit cel	l params.	d(M–M) (Å) <sup>a</sup>		
Composition	a, c (Å)	$V(Å^3)$	<i>Intra</i> layer	<i>Inter</i> layer	
Fe <sub>2</sub> MnSn <sub>2</sub>	5.353	492.24	2.623, 2.731	2.587	
	19.836				
$Fe_{2.5}Mn_{0.5}Sn_2$	5.338	489.46	2.607, 2.777	2.581	
	19.835				
Fe <sub>3</sub> Sn <sub>2</sub> (calc.)	5.327	486.04	2.551, 2.777	2.556	
	19.778				
(exp.)	(5.344	(490.81)	(2.590, 2.754)	(2.590)	
	19.845)				
$Fe_{2.5}Co_{0.5}Sn_2$	5.338	486.92	2.537, 2.791	2.549	
	19.732				
Fe <sub>2</sub> CoSn <sub>2</sub>	5.320	479.33	2.575, 2.745	2.552	
	19.556				

<sup>&</sup>lt;sup>a</sup> The average distances between transition metal atoms.

# 2.2 Magnetic properties of Fe<sub>3-x</sub>M<sub>x</sub>Sn<sub>2</sub>

Results of calculations on the effects of hole and electron doping on the electronic structure of Fe<sub>3</sub>Sn<sub>2</sub> are summarized in Table 2. The FM ground state remains favorable for all substituted compositions, as can be seen from the values of  $\Delta E_{\rm FM-PM}$ , defined as the difference in the calculated total energy of the spin-polarized (FM) and non-spin-polarized (PM) models (the negative value of this difference indicates the stabilization provided by the FM configuration). The relative stability of the FM state decreases only slightly upon substitution of Mn for Fe, but the substitution of Co for Fe causes a substantial decrease in the magnitude of  $|\Delta E_{\rm FM-PM}|$ .

Upon substitution of Mn for Fe (the hole doping), the magnetic moment per Mn atom, m(Mn), increases from 2.35  $\mu_B$  in Fe<sub>2.5</sub>Mn<sub>0.5</sub>Sn<sub>2</sub> to 2.37  $\mu_B$  in Fe<sub>2.M</sub>nSn<sub>2</sub>. Meanwhile, the magnetic moment per Fe atom, m(Fe), initially decreases from 2.24  $\mu_B$  in Fe<sub>3</sub>Sn<sub>2</sub> to 2.16 in Fe<sub>2.5</sub>Mn<sub>0.5</sub>Sn<sub>2</sub>, and then increases to 2.19 in Fe<sub>2</sub>MnSn<sub>2</sub>. This increase in the magnetic moment per Fe atom leads to anomalous behavior of the total moment per f.u., which initially decreases from 6.56  $\mu_B$  in Fe<sub>3</sub>Sn<sub>2</sub> to 6.42  $\mu_B$  in Fe<sub>2.5</sub>Mn<sub>0.5</sub>Sn<sub>2</sub> but then increases to 6.59  $\mu_B$  in Fe<sub>2</sub>MnSn<sub>2</sub>. Magnetic properties of Co-substituted (electron-doped) Fe<sub>3</sub>Sn<sub>2</sub> exhibit an opposite trend, as m(Fe) increases and m(Co) decreases with the increasing Co content. As a result, the total moment per f.u. decreases from 6.03  $\mu_B$  in Fe<sub>2.5</sub>Co<sub>0.5</sub>Sn<sub>2</sub> to 5.21  $\mu_B$  in Fe<sub>2</sub>CoSn<sub>2</sub>.

**Table 2.** Calculated magnetic properties of  $Fe_{3-x}M_xSn_2$  (M = Mn, Co; x = 0.5 and 1.0).

Composition ⇒	Fe <sub>2</sub> MnSn <sub>2</sub>	Fe <sub>2.5</sub> Mn <sub>0.5</sub> Sn <sub>2</sub>	Fe <sub>3</sub> Sn <sub>2</sub>	Fe <sub>2.5</sub> Co <sub>0.5</sub> Sn <sub>2</sub>	Fe <sub>2</sub> CoSn <sub>2</sub>	
Calcd. parameter	1 C <sub>2</sub> IVIII SII <sub>2</sub>	1.62.5141110.53112	1 635112	162.5000.53112	1 C2 C O S 112	
$\Delta E_{\text{FM-PM}}$ , meV/cell	-0.089	-0.093	-0.099	-0.085	-0.074	
$m(M), \mu_B$	2.37	2.35	_	1.04	0.81	
$m(Fe), \mu_B$	2.19	2.16	2.24	2.25	2.26	
$m(Sn)$ , $\mu_B$	-0.08	-0.08	-0.08	-0.06	-0.06	
$m(f.u.), \mu_B$	6.59	6.42	6.56	6.03	5.21	

Examination of the majority- and minority-spin partial DOS (pDOS) curves of the 3d electrons near the Fermi level provides a justification for these observations. In the unsubstituted Fe<sub>3</sub>Sn<sub>2</sub>, the spin polarization leads to the Fermi level falling in a pseudo-gap between the nearly completely populated majority-spin states (shown with red curves in Figure 2) and the minority-spin states (shown with blue curves), a large fraction of which remains depopulated. Such a scenario justifies the stabilization of the FM ground state in this compound. The pDOS curves near the Fermi level exhibit obvious changes in the population of the minority-spin states as the value of x is increased. Substitution of Mn for Fe destabilizes the minority-spin states in Fe<sub>2.5</sub>Mn<sub>0.5</sub>Sn<sub>2</sub> leading

to an increase in moment per f.u. The minority-spin states are further destabilized in  $Fe_2MnSn_2$  while the majority-spin states remain relatively unchanged, further increasing the moment per f.u. (Figures 2a-b). On the other hand, substitution of Co gradually fills the minority states at  $E_F$  contributing to a consistently lower magnetic moment per f.u. with increasing Co content (Figures 2d-e). High-density pDOS peaks indicate localization of electrons leading to high effective masses and low mobility;  $Fe_2MnSn_2$  exhibits the greatest energy dispersion of states, suggesting it may possess the most favorable conductive properties. Indeed, these expectations are confirmed by examination of features in the electronic band structures, which we discuss next.

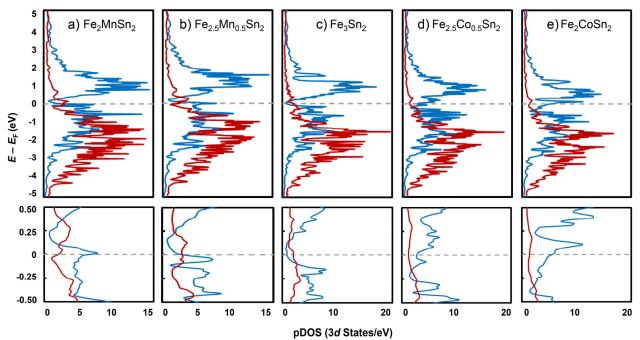


Figure 2. Partial DOS of the majority-spin (red) and minority-spin (blue) 3d electrons of the transition metal sites in Fe<sub>3-x</sub>M<sub>x</sub>Sn<sub>2</sub> (the Fermi level is indicated with a dashed gray line). Expanded plots of the region near  $E_F$  are shown in the bottom panel.

# 2.3 Hole- and electron-doping effects

As already mentioned above, the features observed in the calculated electronic band structure of Fe<sub>3</sub>Sn<sub>2</sub> are comparable to those reported in previous theoretical studies of this compound. Thus, a set of Weyl nodes centered around the

symmetry point  $\Gamma$  is located at  $\sim$ 0.4 eV below  $E_{\rm F}$ , and a set of Dirac points is observed along the V– $\Gamma$ –T k-path at  $\sim$ 0.1 eV below  $E_{\rm F}$  (Figure 3a). These degeneracies are accompanied by high average dispersion of energy bands and large hole pockets at  $\Gamma$ .

The substitution of Mn for Fe has remarkable effects on the electronic band structure. In the case of Fe<sub>2.5</sub>Mn<sub>0.5</sub>Sn<sub>2</sub>, there is a loss of the Dirac points that were observed in Fe<sub>3</sub>Sn<sub>2</sub> at ~0.1 eV below  $E_F$  along the  $\Gamma$ –V and  $\Gamma$ –T lines and an opening gap of ~0.02 eV between the Weyl nodes at ~0.4 eV below  $E_F$  (indicated with red ovals in Figure 3b). A low-dispersion

flatband, however, is observed where these nodes previously resided. Moreover, additional flatbands emerge across the *k*-path at the same energy, and bands below these points exhibit lower average dispersion, consistent with the loss of symmetry and increased localization of the electron wavefunctions.

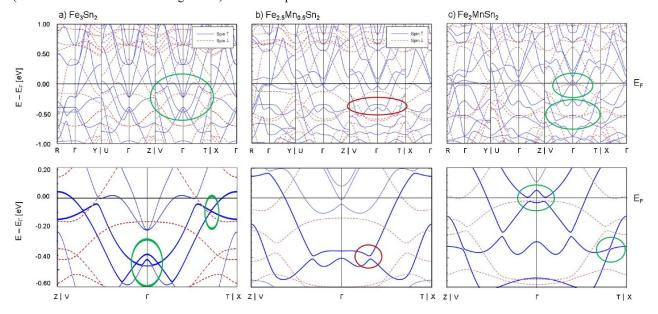
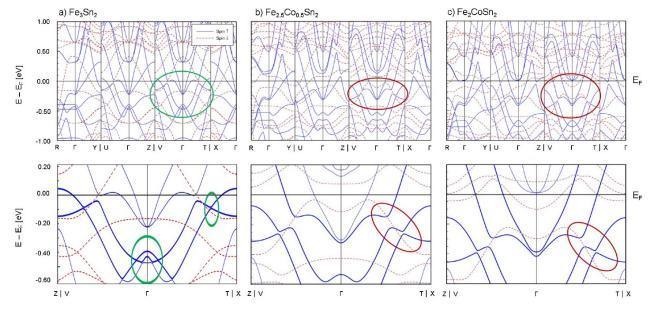


Figure 3. Calculated electronic band structures of  $Fe_{3-x}Mn_xSn_2$ , with enlarged areas near the Fermi level shown in the bottom panel. Degeneracies observed in  $Fe_3Sn_2$  (a) are broken in  $Fe_2.5Mn_{0.5}Sn_2$  (b) but appear to re-emerge in  $Fe_2MnSn_2$  (c) alongside the emergence of new nodal and linear degeneracies at and below  $E_F$ . The solid and dashed curves correspond to the majority-spin and minority-spin states, respectively. The green ovals highlight the desirable degeneracies while the red ones indicate the potential loss of those degeneracies.



**Figure 4.** Calculated electronic band structures of Fe<sub>3-x</sub>Co<sub>x</sub>Sn<sub>2</sub>, with enlarged areas near the Fermi level shown in the bottom panel. Degeneracies observed in Fe<sub>3</sub>Sn<sub>2</sub> (a) are split in Fe<sub>2.5</sub>Co<sub>0.5</sub>Sn<sub>2</sub> (b) and remain non-degenerate in Fe<sub>2</sub>CoSn<sub>2</sub> (c). The solid and dashed curves correspond to the majority-spin and minority-spin states, respectively. The green ovals highlight the desirable degeneracies while the red ones indicate the potential loss of those degeneracies.

Upon further increase in the Mn content, i.e., in Fe<sub>2</sub>MnSn<sub>2</sub>, the degeneracies originally observed in Fe<sub>3</sub>Sn<sub>2</sub> and broken in Fe<sub>2.5</sub>Mn<sub>0.5</sub>Sn<sub>2</sub> appear to re-emerge as potential Weyl-type and Dirac-type points apparent at  $E_{\rm F}$  and  $\sim 0.3$  eV below  $E_{\rm F}$ , respectively (indicated with green ovals in Figure 3c). The emergent Weyl-type cones at  $E_F$  are separated by a gap of ~0.03 eV, and the gap between the former Dirac points at ~0.4 eV below  $E_{\rm F}$  also opens to ~0.03 eV. Nevertheless, a new set of Dirac points emerges approximately 0.05 eV below on either side of these split nodes along the V- $\Gamma$ -T k-path. The appearance of degenerate states and high dispersion in the electronic band structure, most likely, correlate with the more symmetric atomic arrangement in the unit cell of Fe<sub>2</sub>MnSn<sub>2</sub> as compared to that of Fe<sub>2.5</sub>Mn<sub>0.5</sub>Sn<sub>2</sub> (Figure S1). These changes result in greater electron delocalization which promotes increased interaction through FM exchange. Delocalization also facilitates the emergence of degenerate electronic states with potential for high carrier mobility. The expected retention of FM ordering and the high density of degenerate states near E<sub>F</sub> make Fe<sub>2</sub>MnSn<sub>2</sub> a promising candidate for further studies, suggesting that hole-doping of Fe<sub>3</sub>Sn<sub>2</sub>, in general, may yield non-trivial physical properties.

Electronic band structures of Fe3-xCoxSn2 are shown in Figure 4, where the band structure of Fe<sub>3</sub>Sn<sub>2</sub> is also reproduced for the sake of comparison (Figure 4a). As in the case of Fe<sub>2.5</sub>Mn<sub>0.5</sub>Sn<sub>2</sub>, the Dirac points observed for Fe<sub>3</sub>Sn<sub>2</sub> are lost in Fe<sub>2.5</sub>Co<sub>0.5</sub>Sn<sub>2</sub> (Figure 4b), and two sets of cones are open with gaps of 0.01 and 0.07 eV (indicated with red ovals). Lowdispersion bands are observed across the k-path at  $\sim 0.7$  eV below  $E_{\rm F}$ . Further substitution of Co for Fe maintains these energy gaps between the previously degenerate points along the  $\Gamma$ -V and  $\Gamma$ -T lines, as can be seen in the electronic structure of Fe<sub>2</sub>CoSn<sub>2</sub> (Figure 4c), although  $E_F$  is shifted to a higher energy relative to these points, due to filling of the 3d states. Thus, the band structure of Fe<sub>2</sub>CoSn<sub>2</sub> does not exhibit a recovery of emergent degeneracies, as was observed for Fe<sub>2</sub>MnSn<sub>2</sub>. In fact, the 0.01 eV and 0.07 eV gaps between the cones observed in Fe<sub>2.5</sub>Co<sub>0.5</sub>Sn<sub>2</sub> are nearly unaffected in the band structure of Fe<sub>2</sub>MnSn<sub>2</sub>. While nodal degeneracies appear at ~0.9 eV below E<sub>F</sub>, such degeneracies between valence bands are relatively trivial and consistent with the more symmetric atomic arrangement. For both Fe<sub>2.5</sub>Co<sub>0.5</sub>Sn<sub>2</sub> and  $Fe_2CoSn_2$ , the lower average dispersion near  $E_F$ , as compared to that in Fe<sub>3</sub>Sn<sub>2</sub>, indicates reduced carrier mobility with higher effective masses. These results suggest that electron doping does not enhance the magnetic or conductive properties of Fe<sub>3</sub>Sn<sub>2</sub>, but rather suppresses characteristics and removes non-trivial features of the band structure.

# 3. Concluding Remarks

Our theoretical investigation clearly reveals the immediate impact of hole- and electron-doping substitutions on the

magnetic and electronic properties of frustrated kagomé ferromagnet Fe<sub>3</sub>Sn<sub>2</sub>. Hole-doping through substitution of Mn for Fe initially breaks the nodal degeneracies observed in Fe<sub>3</sub>Sn<sub>2</sub>, but at higher Mn content such degeneracies re-emerge. Especially interesting is the appearance of nearly degenerate Weyl points at the Fermi level, which could lead to exotic conducting and magnetic properties. The retention and emergence of degenerate states might indicate strong coupling between the electronic and spin degrees of freedom in the kagomé lattice, which could result both in anomalous transport effects and multiple magnetic ground states with non-collinear spin textures. In contrast, electron doping eliminates the nodal degeneracies and does not lead to appearance of any re-emergent features of interest in the electronic band structure. Thus, we conclude that the present study identifies Fe<sub>3-x</sub>Mn<sub>x</sub>Sn<sub>2</sub> as a suitable candidate for further investigations of magnetic and topological properties of Fe<sub>3</sub>Sn<sub>2</sub>-based kagomé metals. Experimental studies of such hole-doping effects are currently under way in our laboratories, and their results will be reported in due course.

# Acknowledgements

This work was supported by the National Science Foundation (award DMR-1905499 to M.S.). The computing for this project was performed on the HPC cluster at the Research Computing Center at the Florida State University.

# **Conflict of Interest Statement**

There are no conflicts of interest to declare.

# Data availability statement

All computational data discussed in this work are available freely at https://github.com/shatruk-fsu/Fe3-xMxSn2.

## References

- [1] Ramirez A P 1994 Annu. Rev. Mater. Sci. 24 453-80
- [2] Greedan J E 2001 J. Mater. Chem. 11 37-53
- [3] Balents L 2010 Nature 464 199-208
- [4] Balz C et al. 2016 Nat. Phys. 12 942-9
- [5] Hashizume Y and Suzuki M 2011 Int. J. Mod. Phys. B 25 3529-38
- [6] Kaufmann J, Steiner K, Scalettar R T, Held K and Janson O 2021 Phys. Rev. B 104 165127
- [7] Canfield P C and Bud'ko S L 2016 Rep. Prog. Phys. 79 084506
- [8] Jain A, Yusuf S M, Kanoo P, Dhar S K and Maji T K 2020 Phys. Rev. B 101 140413
- [9] Kang S H and Lee K 2013 Acta Mater. 61 952-73
- [10] Yin J-X et al. 2018 Nature 562 91-5
- [11] Liu Z, Liu F and Wu Y-S 2014 Chin. Phys. B 23 077308
- [12] Mielke A 1992 J. Phys. A 25 4335-45
- [13] Tasaki H 1992 Phys. Rev. Lett. 69 1608-11
- [14] Imada M and Kohno M 2000 Phys. Rev. Lett. 84 143-6

- [15] Zhang H, Feng H, Xu X, Hao W and Du Y 2021 Adv. Quant. Technol. 4 2100073
- [16] Kida T, Fenner L A, Dee A A, Terasaki I, Hagiwara M and Wills A S 2011 *J. Phys. Condens. Matter* 23 112205
- [17] Ye L et al. 2018 Nature 555 638-42
- [18] Hou Z et al. 2018 Nano Lett. 18 1274-9
- [19] Malaman B, Roques B, Courtois A and Protas J 1976 Acta Crystallogr. Sect. B 32 1348-51
- [20] Fenner L A, Dee A A and Wills A S 2009 J. Phys. Condens. Matter 21 452202
- [21] Lin Z et al. 2018 Phys. Rev. Lett. 121 096401
- [22] Elding-Pontén M, Stenberg L, Larsson A-K, Lidin S and Ståhl K 1997 J. Solid State Chem. 129 231-41
- [23] Fjellvaag H and Kjekshus A 1986 Acta Chem. Scand. Ser. A A40 23-30
- [24] Recour Q, Ban V, Gercsi Z, Mazet T, François M and Malaman B 2013 Phys. Rev. B 88 054429
- [25] Giannozzi P et al. 2009 J. Phys. Condens. Matter 21 395502
- [26] Perdew J P, Burke K and Ernzerhof M 1996 Phys. Rev. Lett. 77 3865-8
- [27] Momma K and Izumi F 2011 J. Appl. Cryst. 44 1272-6
- [28] Fayyazi B et al. 2019 Acta Mater. 180 126-40
- [29] Malaman B, Fruchart D and Caer G L 1978 J. Phys. F 8 2389

# **Supporting Information**

# Effect of electron- and hole-doping on properties of kagomé-lattice ferromagnet Fe<sub>3</sub>Sn<sub>2</sub>

# Milo Adams<sup>1</sup>, Chen Huang<sup>2,3,4,\*</sup> and Michael Shatruk<sup>1,3,4,\*</sup>

E-mail: shatruk@chem.fsu.edu and chuang3@fsu.edu

Table S1. Energies of different atomic configurations for Fe <sub>2.5</sub> M <sub>0.5</sub> Sn <sub>2</sub> (M = Mn, Co)	S
Figure S1. Relaxed structures of Fe <sub>3-x</sub> M <sub>x</sub> Sn <sub>2</sub> shown the substitution patterns	
Table S2. Distribution of Fe and Mn atoms in the relaxed Fe <sub>3-x</sub> Mn <sub>x</sub> Sn <sub>2</sub> structures	
Table S3. Distribution of Fe and Co atoms in the relaxed Fe <sub>3-x</sub> Co <sub>x</sub> Sn <sub>2</sub> structures	S3
Table S4. Average Fe-Sn and Sn-Sn bond lengths in the optimized structures of Fe <sub>2-x</sub> M <sub>x</sub> Sn <sub>2</sub>	

**Table S1.** Energies of different atomic configurations for  $Fe_{2.5}M_{0.5}Sn_2$  (M = Mn, Co) relative to the ground state at 0 eV as a function of substituting the Mn or Co atom for different crystallographic sites of Fe in the primitive unit cell.

		$E_{\rm total}~({ m meV})$			
Site <sup>a</sup>		Mn	Co		
1	<i>-y, x-y, z</i>	0.0071	0.0041		
2	-x, -y, -z	0.0000	0.0036		
3	x, y, z	0.0005	0.0019		
4	-x+y, -x, z	0.0007	0.0031		
5	x-y, x, -z	0.0033	0.0022		
6	y, -x+y, -z	0.0027	0.0000		

<sup>&</sup>lt;sup>a</sup> The coordinate labels of six sites correspond to the symmetry-related positions of Fe atoms in the original hexagonal unit cell of Fe<sub>3</sub>Sn<sub>2</sub>.

<sup>&</sup>lt;sup>1</sup> Department of Chemistry and Biochemistry, Florida State University, Tallahassee, FL 32306-4390, USA

<sup>&</sup>lt;sup>2</sup> Department of Scientific Computing, Florida State University, Tallahassee, FL 32306-4120, USA

<sup>&</sup>lt;sup>3</sup> Materials Science and Engineering Program, Florida State University, Tallahassee, FL 32310, USA

<sup>&</sup>lt;sup>4</sup> National High Magnetic Field Laboratory, Tallahassee, FL 32310, USA

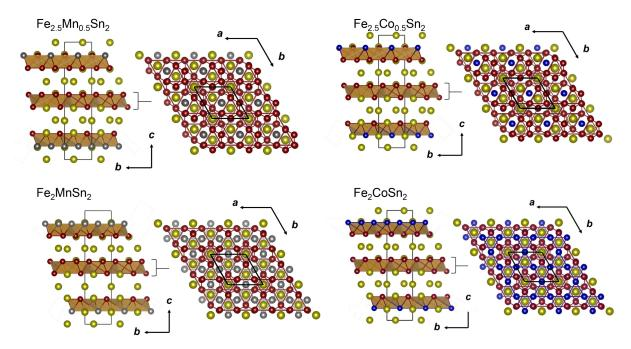


**Figure S1.** Relaxed structures of  $Fe_{3-x}M_xSn_2$  viewed down the *a* axis (left) to show the stacking of layers, and down the *c* axis (right) to show the top view of the kagomé layer. Color scheme: Fe = garnet, Sn = gold, Fe = garnet, Fe = garnet,

**Table S2.** An example configuration of Fe and Mn atoms in the relaxed Fe<sub>3-x</sub>Mn<sub>x</sub>Sn<sub>2</sub> unit cell for Mn substitution in Site 2 (Table S1), as determined by DFT calculations. The positions are given as fractional coordinates.

Fe <sub>2.5</sub> Mn <sub>0.5</sub>	$\operatorname{Sn}_2$		
Atom	x	у	Z
Mn1	0.4972	0.5071	0.1130
Mn2	0.5074	0.4962	0.8866
Mn3	0.4968	0.9913	0.1126
Fe1	0.5105	0.0166	0.8860
Fe2	0.0167	0.5093	0.1133
Fe3	0.9868	0.4930	0.8865
Fe4	0.1579	0.8401	0.4473
Fe5	0.1687	0.8237	0.2206
Fe6	0.1579	0.3175	0.4473
Fe7	0.1688	0.3465	0.2207
Fe8	0.6802	0.8400	0.4475
Fe9	0.6468	0.8242	0.2217
Fe10	0.8279	0.1736	0.7804
Fe11	0.8399	0.1584	0.5531
Fe12	0.8278	0.6508	0.7790
Fe13	0.8401	0.6808	0.5530
Fe14	0.3506	0.1737	0.7789
Fe15	0.3179	0.1584	0.5529
Sn1	0.0011	0.0015	0.1054
Sn2	0.0032	0.0001	0.8939
Sn3	0.6655	0.3325	0.4388

Sn4	0.6629	0.3319	0.2282	Sn4	0.6667	0.3333	0.2296
Sn5	0.3346	0.6665	0.7717	Sn5	0.3333	0.6667	0.7704
Sn6	0.3325	0.6657	0.5616	Sn6	0.3333	0.6667	0.5611
Sn7	-0.0024	-0.0010	0.3312	Sn7	1.0000	1.0000	0.3313
Sn8	0.0002	-0.0006	0.6691	Sn8	1.0000	1.0000	0.6688
Sn9	0.6678	0.3326	0.6634	Sn9	0.6667	0.3333	0.6627
Sn10	0.6689	0.3356	0.0023	Sn10	0.6667	0.3333	0.0019
Sn11	0.3359	0.6689	0.9970	Sn11	0.3334	0.6667	0.9980
Sn12	0.3299	0.6653	0.3370	Sn12	0.3334	0.6667	0.3373

**Table S3.** An example configuration of Fe and Mn atoms in the relaxed  $Fe_{3-x}Co_xSn_2$  unit cell for Co substitution in Site 2 (Table S1), as determined by DFT calculations. The positions are given as fractional coordinates.

Fe <sub>2.5</sub> Co <sub>0.5</sub>	$Sn_2$			Fe <sub>2</sub> CoSn <sub>2</sub>			
Atom	$\boldsymbol{x}$	y	z	Atom	$\boldsymbol{x}$	y	z
Co1	0.4970	0.5048	0.1102	Col	0.4947	0.5053	0.1098
Co2	0.5072	0.5025	0.8906	Co2	0.5053	0.4947	0.8902
Co3	0.4966	0.9976	0.1104	Co3	0.4947	0.9893	0.1098
Fe1	0.5145	0.0210	0.8865	Co4	0.5053	0.0107	0.8902
Fe2	0.0291	0.5174	0.1161	Co5	0.0107	0.5053	0.1098
Fe3	0.9876	0.4940	0.8862	Co6	0.9893	0.4947	0.8902
Fe4	0.1566	0.8388	0.4467	Fe1	0.1597	0.8403	0.4464
Fe5	0.1597	0.8212	0.2192	Fe2	0.1742	0.8258	0.2155
Fe6	0.1570	0.3159	0.4468	Fe3	0.1597	0.3193	0.4464
Fe7	0.1590	0.3421	0.2192	Fe4	0.1742	0.3484	0.2155
Fe8	0.6767	0.8370	0.4469	Fe5	0.6807	0.8403	0.4464
Fe9	0.6362	0.8206	0.2164	Fe6	0.6516	0.8258	0.2155
Fe10	0.8348	0.1745	0.7808	Fe7	0.8258	0.1742	0.7845
Fe11	0.8393	0.1561	0.5533	Fe8	0.8403	0.1597	0.5536
Fe12	0.8373	0.6518	0.7820	Fe9	0.8258	0.6516	0.7845
Fe13	0.8384	0.6786	0.5532	Fe10	0.8403	0.6807	0.5536
Fe14	0.3558	0.1713	0.7822	Fe11	0.3484	0.1742	0.7845
Fe15	0.3185	0.1579	0.5530	Fe12	0.3193	0.1597	0.5536
Sn1	-0.0004	0.0028	0.1041	Sn1	0.0000	0.0000	0.1011
Sn2	0.0055	0.0039	0.8962	Sn2	0.0000	0.0000	0.8989
Sn3	0.6643	0.3308	0.4383	Sn3	0.6667	0.3333	0.4374
Sn4	0.6497	0.3273	0.2243	Sn4	0.6667	0.3333	0.2211
Sn5	0.3451	0.6639	0.7736	Sn5	0.3333	0.6667	0.7789
Sn6	0.3313	0.6642	0.5618	Sn6	0.3333	0.6667	0.5626
Sn7	-0.0088	-0.0042	0.3298	Sn7	0.0000	0.0000	0.3281
Sn8	0.0028	-0.0019	0.6701	Sn8	0.0000	0.0000	0.6719
Sn9	0.6715	0.3323	0.6647	Sn9	0.6667	0.3333	0.6666
Sn10	0.6719	0.3405	0.0035	Sn10	0.6667	0.3333	0.0019
Sn11	0.3421	0.6749	0.9986	Sn11	0.3333	0.6667	0.9981
Sn12	0.3238	0.6627	0.3352	Sn12	0.3333	0.6667	0.3334

**Table S4.** Average Fe-Sn and Sn-Sn bond lengths in the optimized structures of Fe<sub>3-x</sub> $M_x$ Sn<sub>2</sub>, demonstrating that the more pronounced changed of the unit cell along the c axis is caused mainly by changes in the interlayer Fe-Sn distances.

	In-Plane Dis	tances (Å)	Interlayer Distances (Å)			
	d(Sn-Sn)	d(Fe–Sn	d(Fe-Sn)	d(Fe–Sn)		
	honeycomb	kagomé	kagomé-kagomé	kagomé-honeycomb		
Fe <sub>2</sub> MnSn <sub>2</sub>	3.093	2.682	2.794	2.712, 2.731		
$Fe_{2.5}Mn_{0.5}Sn_2$	3.082	2.673	2.789	2.716, 2.738		
Fe <sub>3</sub> Sn <sub>2</sub> Calcd.	3.077	2.671	2.783	2.721, 2.735		
(Exp.)	(3.086)	(2.679)	(2.799)	(2.727, 2.731)		
$Fe_{2.5}Co_{0.5}Sn_2$	3.077	2.676	2.773	2.724, 2.754		
Fe <sub>2</sub> CoSn <sub>2</sub>	3.073	2.666	2.767	2.728, 2.732		